Medical Engineering and Physics 88 (2021) 69–77

Contents lists available at ScienceDirect

Medical Engineering and Physics

journal homepage: www.elsevier.com/locate/medengphy

Impact of surgical alignment, tray material, PCL condition, and patient anatomy on tibial strains after TKA

Huizhou Yang, Riza Bayoglu, Chadd W. Clary, Paul J. Rullkoetter*

Center for Orthopaedic Biomechanics, University of Denver, 2155 E. Wesley Ave., Denver, CO 80208, USA

ARTICLE INFO

Article history:
Received 6 August 2020
Revised 4 December 2020
Accepted 5 January 2021

Keywords:
Knee arthroplasty
Bone remodeling
Cemented
Strain energy density
Finite element analysis

ABSTRACT

Bone remodeling after total knee arthroplasty is regulated by the changes in strain energy density (SED), however, the critical parameters influencing post-operative SED distributions are not fully understood. This study aimed to investigate the impact of surgical alignment, tray material properties, posterior cruciate ligament (PCL) balance, tray posterior slope, and patient anatomy on SED distributions in the proximal tibia.

Finite element models of two tibiae (different anatomy) with configurations of two implant materials, two surgical alignments, two posterior slopes, and two PCL conditions were developed. The models were tested under the peak loading conditions during gait, deep knee bending, and stair descent. For each configuration, the contact forces and locations and soft-tissue loads of interest were taken into consideration. SED in the proximal tibia was predicted and the changes in strain distributions were compared for each of the factors studied.

Tibial anatomy had the most impact on the proximal bone SED distributions, followed by PCL balancing, surgical alignment, and posterior slope. In addition, the thickness of the remaining cortical wall after implantation was also a significant consideration when evaluating tibial anatomy. The resulting SED changes for alignment, posterior slope, and PCL factors were mainly due to the differences in joint and soft-tissue loading conditions. A lower modulus tray material did result in changes in the post-operative strain state, however, these were almost negligible compared to that seen for the other factors.

1. Introduction

Total knee arthroplasty (TKA) relieves pain and restores function in patients with advanced knee osteoarthritis [1], and the future demand in knee arthroplasty is predicted to grow by 85%, to 1.26 million procedures by 2030 [2]. One of the most common complications and hence reason for revision is mechanical loosening (23.1% of all revised TKA) [3]. It is known that bone remodels in response to applied loads by changing its architecture [4,5], and this bone remodeling process after TKA is regulated by the changes in strain energy density (SED) [6]. The recruitment of osteoclasts and osteoblasts is controlled by the SED-related signals sent through the osteocytic-canalicular network [7]. Insufficient stimuli as a result of stress shielding can promote bone resorption and potential for aseptic loosing of the implant. Hence, it is essential to identify the critical parameters influencing post-operative SED distributions.

In general, the strain state inside the tibia cannot be measured experimentally. Finite element methods have been previously used to evaluate factors affecting post-operative tibial strain states [8]. Studies have investigated the impact of stem length, implant material and alignment, fixation method (cemented & cementless), and tray-bone fit with cadaveric or synthetic tibial models under pure body weight, single activity, or multi-activity static loading conditions [9–13]. Testing loads have been typically applied uniformly on the surface of the polyethylene insert or tibial plateau, without additional soft-tissue loading on the tibia. Perillo-Marcone, et al. showed that the stresses generated within the implanted tibia were dependent on the kinematics of the joint (e.g. contact locations), which are affected by the TKR design, surgical alignment, and the balance of the soft tissue [14]. Also, a larger influence of the muscle loading on the strain distribution was unveiled by Duda, et al., which was rarely considered in previous studies [15].

To our knowledge, none of the previous studies considered both femoral-insert contact (contact locations and force directions) and soft tissue loading conditions (tendon and ligament forces and di-

* Corresponding author.
E-mail address: paul.rullkoetter@du.edu (P.J. Rullkoetter).

https://doi.org/10.1016/j.medengphy.2021.01.001
1350-4533/

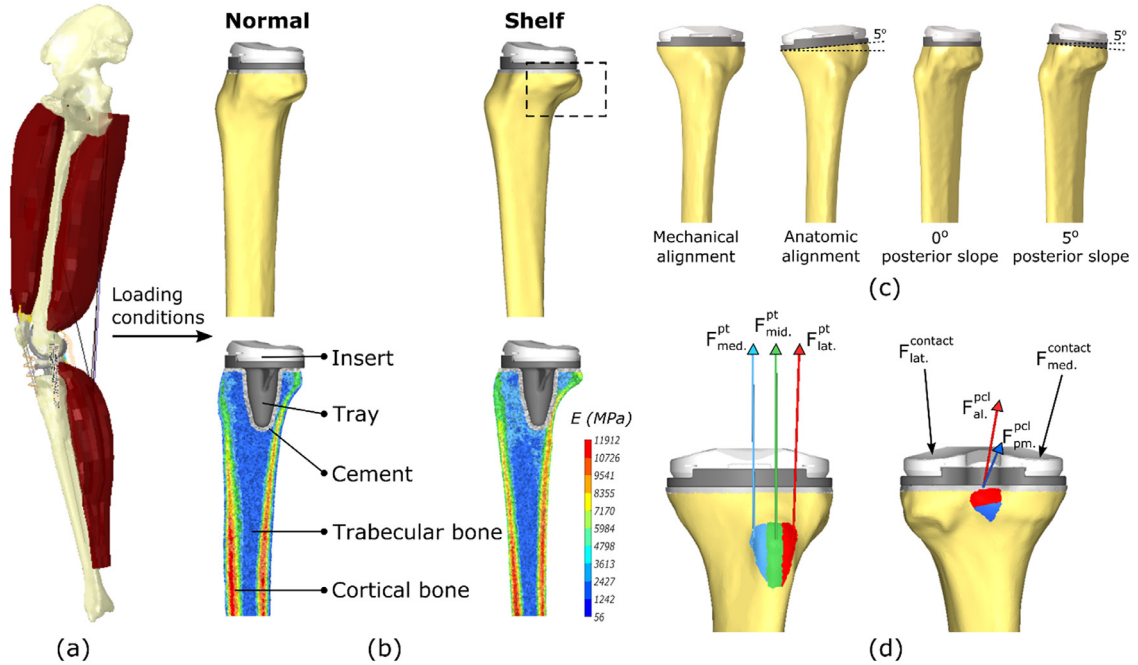

Fig. 1. Model set up. (a) Lower limb finite element model for estimation of joint and soft tissue loads applied to deformable tibial models. (b) Young's modulus distributions in the cortical and trabecular tibia bone for the normal and shelf tibiae. (c) The tibial models with different alignment and tray posterior slopes. (d) Patellar tendon, PCL sub-bundles, and their attachment sites. External boundary conditions, including joint contact forces and ligament forces. (F^{pt}_{med}= medial patellar tendon bundle force; $F^{pcl}_{al.}$= anterolateral PCL bundle force; $F^{contact}_{med}$= medial femoral-insert contact force; similar for the rest). ***(color should be used for this figure)***.

rections) when investigating bone strains. The objective of the current study is to investigate the influence of surgical alignment, tray material properties, posterior cruciate ligament (PCL) balance, tray posterior slope, and patient anatomy on proximal tibial strain energy density while considering physiological femoral-insert contact conditions and patellar and PCL ligament forces. We virtually implanted two distinct tibiae using different alignment methods, tray posterior slopes, and tray materials. Computational models were tested under peak compressive stance phase gait (GT), deep knee bending (DKB), and stair descent (SD) loading conditions which were individually determined for each model configuration. A nominal and a tight PCL condition were also taken into consideration. The strain energy density in the proximal tibia was predicted for those models and compared for each of the factors studied, with a focus on the change in strain distribution for each factor.

2. Methods

2.1. Finite element models of the tibia

Three-dimensional geometries of two intact left tibiae, one typical and one with larger posterior overhang (subsequently indicated as 'shelf' tibia) (Fig. 1b) were manually segmented using ScanIP (Simpleware, Exeter, UK) from computed tomography (CT) scans. The images were in DICOM format with a 0.6-mm slice thickness and a maximum 0.87-mm pixel spacing. The studied tibiae were similar in size to ensure the same tray size fit. However, the shelf tibia selected had the most extreme posterior overhang variation out of a database of 170 specimens. The cortical wall thickness of the normal tibia was slightly larger than the shelf tibia with varying magnitude along its length (less than 1 mm with differences increasing inferiorly). Each tibial geometry was constructed into a solid model and was virtually implanted with a cemented prosthesis (size 5, fixed-bearing, cruciate-retaining, Attune®, DePuy Synthes, Warsaw, IN) using mechanical and anatomic alignment techniques with both 0 and 5-degree posterior slopes in HyperMesh (Altair Engineering Inc., Troy, Michigan) (Fig. 1c). However, it should be understood by the reader that, according to the manufacturer's surgical technique, a posterior slope of 0° is outside the range of 5 – 7° recommended for the cruciate retaining version of Attune to provide proper PCL tension. It should be noted that a size 5 tray was always the best-fit or suitable in each resection scenario with regard to the surgical approach. The surgical alignment techniques used in this study were: 3° femoral external rotation, 0° varus slope, and 0° hip-knee-ankle (HKA) angle for mechanical alignment; 0° femoral external rotation, 5° varus slope, and 3° HKA angle for anatomic alignment. The technique for placement of the tray (determining the anterior/posterior location and internal/external rotation relative to the tibia) was done using a virtual implantation algorithm and unchanged across all resection scenarios. A 2-mm-thick cement layer was created between the tibial tray and bone [16]. The proximal 150-mm tibial geometry was represented in the finite element simulations. The polyethylene insert, tibial tray, cement layer, and the bone were meshed with 1-mm, linear tetrahedral elements, which were identified from a mesh convergence study. All components were modeled as linearly elastic and with different material properties (Table 1). Two common metal materials for the tibia tray, cobalt-chrome (CoCrMo) and titanium alloy (Ti6Al4V) were considered. Heterogeneous material properties of the tibiae were calculated from the CT Hounsfield units and were assigned to each tibia element using an in-house mapping software. Previously established relationships were used for calculating the apparent bone density and elastic modulus for the individual elements [18, 19]. Around 400 material properties (1 property per 4 mg/cm^3 bone apparent density) were used for modeling the tibiae based on a prior convergence study. The bone-cement and cement-tray interfaces were assumed to be fully bonded. The interface between the polyethylene insert and metal tray was modeled as a contact pair with a friction coefficient of 0.04. The distal ends of the tibial models were fully fixed.

Table 1
Material properties used in the computational models.

Component/Material	Density (g/cm^3)	Elastic moduli (MPa)	Poisson's ratio
Insert - UHMWPE	0.94	691	0.45
Tray - CoCrMo	8.50	210,000	0.30
Tray - Ti6Al4V	4.50	105,000	0.27
Cement - PMMA	2.00	2551	0.40
Cortical bone	$1 \leq \rho \leq 1.9$*	$3290 \leq E \leq 11{,}912$	0.30
Trabecular bone	$0.1 \leq \rho < 1$	$56 \leq E < 3290$	0.30

* 1.9 g/cm^3 was the maximum density of the tibiae used in this study. The corresponding elastic modulus was 11,912 MPa. The values were in range with the human tibial density and elastic properties reported in literature [17].

The effect of the PCL forces on the tibial strain state was assessed. Patellar and PCL ligaments were divided into sub-bundles and modeled as connector elements, using three bundles to represent the patella tendon (lateral, central, and medial bundles) and two for the PCL (anterolateral and posteromedial bundles). The attachment sites of these ligament bundles on the tibia were reconstructed based on the anatomy of each tibia (Fig. 1d).

Additional models were built for the shelf tibia (initially has lower mean material properties) with material properties matched to the normal tibia to best isolate the impact of tibial geometry on bone strains. This was achieved by modifying the apparent density range of the shelf tibia to be the same as the normal tibia and recalculating Young's moduli based on the new bone apparent density for each element.

2.2. External boundary conditions

The loading and boundary conditions applied to the models were determined using a previously-developed finite element lower limb model (Fig. 1a) [20]. The function of this simulation was to assess implant mechanics during simulated activities under multi-factorial sources of variability, including soft tissue, surgical technique and alignment variability. The lower limb model includes a vertical load applied at the hip, quadriceps and hamstring loading, M-L load at the ankle, an I-E torque about the long axis of the tibia, and A-P motion of the pelvis. In the simulation, proportional-integral-derivative (PID) control is used with the quadriceps actuator to achieve a desired flexion profile. The external loading conditions were developed using data from the orthoload telemetric joint loading measurements [21]. Using the geometry of the telemetric implant, the external loading conditions were derived to best reproduce the average measured, 6°-of-freedom joint loading. Subsequently, implant design and alignments have been studied with these consistent external boundary conditions (see reference 20 for complete description).

The implant design used in this study was incorporated into the lower limb model to simulate GT, DKB, and SD activities in Abaqus/Explicit (SIMULIA, Providence, RI). The initial strains of the PCL bundles (nominal PCL condition) were calibrated by matching the elongations and tensions of the PCL bundles, and medial and lateral femoral-insert AP translations with literature [22–24]. A tight PCL condition was then defined by increasing the initial strain of each bundle by 5%, which made the resulting PCL tension and femoral-insert AP translation still within reported ranges but approaching the boundary. Subsequently, eight unique configurations (two surgical alignments, two tray posterior slopes, and two PCL conditions) were incorporated into the lower limb model to simulate the aforementioned activities. Peak femoral-insert contact forces and locations and corresponding ligament force and directions were extracted from the lower limb model and applied to the models for bone strain analysis. The variables of tray material and tibial anatomy were not included in the lower limb model since these variables had negligible impact on the target outputs (contact forces and locations; ligament forces and directions). It should be noted that for each activity, the peak loads always occurred at the same frame no matter which alignment, tray posterior slope, and PCL conditions were used.

2.3. Analysis

In total, 144 finite element simulations (two tibiae, two tray materials, two surgical alignments, two posterior slopes, two PCL conditions, three activities, and additional models for the shelf tibia) were run in Abaqus/Standard.

The SED in the proximal 50-mm of the tibia was predicted for each model configuration. The proximal tibia was subdivided into four regions-of-interest (ROI): medial-proximal (MP), lateral-proximal (LP), medial-distal (MD) and lateral-distal (LD) (Fig. 3) [25]. For each activity, the changes in SED distributions were compared for each of the factors studied. For example, when studying the impact of alignment technique during DKB activity, all the models with mechanical alignment (24 models) were compared with their counterparts with anatomic alignment (24 models) while all other factors were the same. The total strain energy in each ROI was calculated and normalized with respect to tibial regional volumes (which were slightly different due to the variations of the resection plane when introducing different surgical alignments and tray posterior slopes), then compared between those comparative models. The impact of a factor was then calculated by averaging the percent changes in the strain states of the comparison pairs (Fig. 4). The relationship between the factors studied and the SED response was evaluated by using the multi-factor ANOVA (analysis of variance) statistical method. The P-value and contribution of each factor were reported in Table 3. The contribution was calculated as the percentage that each source contributes to the total sequential sums of squares (Seq SS). In this study, Seq SS quantifies the amount of variation in SED response that is explained by each term. Thus, the contribution can be used as an indicator which evaluates the weight of the impact on SED variations for each factor. It should be noted that the sequential SS and the adjusted SS were the same since the design matrix in this study is orthogonal. Thus, the order of the factors entered into the regression model has no impact on the ANOVA results.

In addition to the absolute strain predictions, comparison plots of the SED *difference* were created to better understand the changes in distributions inside the proximal tibia. For each factor studied, the SED of each tibial element was compared with the closest element in the counterpart model. Nine tibial sections parallel to the frontal plane, from anterior to posterior, were made to visualize the SED changes inside the tibia (Fig. 5). To best understand the impact of tibial geometry, representative plots of the *absolute* SED distributions inside the bone were made for the normal and shelf tibia (Fig. 6).

Table 2
External boundary conditions derived and applied to the computational models (al. bundle = anterolateral bundle; pm. bundle = posteromedial bundle).

Peak loading conditions during gait stance phase (N)				
Component	**0° posterior slope Mechanical alignment**	**0° posterior slope Anatomic alignment**	**5° posterior slope Mechanical alignment**	**5° posterior slope Anatomic alignment**
Med. Contact	1334.9	1603.6	1284.5	1566.8
Lat. Contact	1084.5	797.5	1086.2	793.4
Patellar tendon lat.	628.4	662.7	598.2	626.1
Patellar tendon mid.	745.1	758.6	786.2	799.1
Patellar tendon med.	495.0	435.1	434.1	379.2
PCL al. bundle	slack	slack	slack	slack
PCL pm. bundle	slack	slack	slack	slack
Peak loading conditions during deep knee bending (N)				
Component	**0° posterior slope Mechanical alignment (Tight/Nominal PCL)**	**0° posterior slope Anatomic alignment (Tight/nominal PCL)**	**5° posterior slope Mechanical alignment (Tight/Nominal PCL)**	**5° posterior slope Anatomic alignment (Tight/Nominal PCL)**
Med. Contact	461.6/394.5	112.8/161.2	442.7/425.0	242.5/297.0
Lat. Contact	1904.7/1796.7	2274.4/2055.0	1774.7/1632.4	2005.6/1782.5
Patellar tendon lat.	slack/slack	98.12/80.8	slack/slack	81.7/65.5
Patellar tendon mid.	1162.6/1142.8	1219.7/1203.7	1167.0/1146.3	1234.4/1224.6
Patellar tendon med.	581.2/654.1	333.0/422.1	558.5/632.4	338.9/414.6
PCL al. bundle	540.2/326.2	596.0/376.6	390.3/166.3	439.3/196.1
PCL pm. bundle	slack/slack	slack/slack	slack/slack	slack/slack
Peak loading conditions during stair descent (N)				
Component	**0° posterior slope Mechanical alignment**	**0° posterior slope Anatomic alignment**	**5° posterior slope Mechanical alignment**	**5° posterior slope Anatomic alignment**
Med. Contact	1584.2	1962.0	1575.4	1955.6
Lat. Contact	1591.9	1212.4	1543.1	1162.1
Patellar tendon lat.	709.1	760.7	672.3	717.7
Patellar tendon mid.	915.7	944.3	948.5	973.3
Patellar tendon med.	741.1	649.0	680.4	600.0
PCL al. bundle	slack	slack	slack	slack
PCL pm. bundle	slack	slack	slack	slack

3. Results

3.1. Convergence study

For mesh convergence, tibial elements were analyzed with 1.5, 1.0, and 0.75-mm element edge lengths. For defining material properties of the tibiae, 100, 200, 300, and 400 material properties were evaluated. The differences between the predicted SED in the proximal tibia when using 1.0 and 0.75-mm mesh sizes were less than 5%, and hence1.0 mm meshes were used for the analyses presented. The SED differences between using 100 and 400 material cards were less than 1.5%.

3.2. Lower limb simulations

The inputs (femoral-insert and ligament forces and locations) to individual bone strain models were derived from the lower limb models and shown in Fig. 2& Table 2. For GT and SD activities, the PCL remained slack at the peak loading frame even if the PCL was pre-tightened. Thus, the two PCL conditions used in this study will not affect bone strain for these activities.

3.3. Relative changes in strain distribution

The sensitivity of SED in each tibial region to each of the five factors was determined (Fig. 4). The average changes in SED (1.1%, 2.6%, 1.1%) (GT, DKB, and SD, respectively) over all the regions associated with the change in tray material were much smaller than that seen with the changes in PCL balance (N/A, 25.0%, N/A) (GT, DKB, and SD), surgical alignment (23.0%, 15.3%, 24.4%), posterior slope (11.3%, 18.7%, 8.7%), and tibial anatomy (24.0%, 18.0%, 22.1%). PCL balance did not have an impact for GT and SD cases since the PCL bundles were slack at the peak tibio-femoral compressive loading frames for those two activities. Tibial anatomy had the largest impact on proximal bone SED distributions, followed by PCL balancing, surgical alignment, tray posterior slope, and material (Table 3). Representative contour maps of the SED changes within the tibia are shown in Fig. 5. The contoured, comparative SED results reveal where the strain differences occur with change in each factor.

The tibial geometry had the largest impact on the strain states although the bone volume and material differences between tibiae were considered (by comparing normal tibia with shelf tibia models which have the same mean material properties). When comparing the shelf tibia with the normal tibia, SED decreased mostly at the distal regions (−34.2% for GT; −26.8% for DKB; −29.3% for SD), whereas the changes in proximal regions were relatively smaller (13.8% for GT; 9.1% for DKB; 14.8% for SD) (Fig. 4).

The initial PCL tension influenced the strain distributions in the proximal tibia significantly during DKB activity, a 5% tightened PCL resulted in increased SED distributions over all the regions (+20.1% in MP; +32.9% in LP; +32.7% in MD; +14.1% in LD) (Fig. 5b).

Surgical alignment (indicated frontal plane alignment and HKA angle here) of the tray had a considerable effect on the strain states. For GT and SD activities, less SED was calculated in the medial regions (both MP and MD) (−26.0% for GT; −24.5% for SD) for the mechanical alignment case compared anatomic alignment case, whereas more SED was observed in the lateral regions (+14.9% for GT; +21.3% for SD) (Figs. 4 and 5c). For DKB activity, the SED decreased over all regions (−17.5% in MP; −10.9% in LP; −12.2% in MD; −10.8% in LD) (Figs. 4 and 5d).

In all the activities, we found that the SED increased posteriorly and decreased anteriorly when introducing a tray posterior slope (Fig. 5e). For DKB activity specifically, the SED decreased over all

Table 3
P-value and contributions of each factor on changes in SED distributions (MP: medial-proximal; LP: lateral-proximal; MD: medial-distal; LD: lateral-distal).

		P-values				**Factor contributions**				
	Source	MP	LP	MD	LD	MP	LP	MD	LD	**Average**
GT	Surgical alignment	0.004	0.000	0.000	0.049	22.92%	81.13%	33.51%	1.16%	**34.68%**
	Posterior slope	0.002	0.022	0.058	0.004	29.34%	6.89%	1.69%	3.17%	**10.27%**
	Tray material	0.632	0.863	0.850	0.897	0.43%	0.03%	0.01%	0.00%	**0.12%**
	Tibia anatomy	0.002	0.284	0.000	0.000	28.04%	1.23%	60.60%	93.06%	**45.73%**
DKB	PCL balance	0.000	0.000	0.000	0.000	25.92%	35.41%	30.10%	7.00%	**24.61%**
	Surgical alignment	0.000	0.000	0.001	0.000	32.81%	8.13%	10.58%	5.70%	**14.31%**
	Posterior slope	0.000	0.000	0.000	0.000	19.35%	45.50%	27.52%	4.33%	**24.18%**
	Tray material	0.910	0.019	0.597	0.726	0.01%	1.82%	0.22%	0.02%	**0.52%**
	Tibia anatomy	0.003	0.033	0.001	0.000	6.35%	1.49%	11.83%	78.64%	**24.58%**
SD	Surgical alignment	0.001	0.000	0.000	0.922	36.86%	82.99%	38.81%	0.00%	**39.67%**
	Posterior slope	0.001	0.211	0.341	0.157	34.01%	1.04%	0.30%	0.73%	**9.02%**
	Tray material	0.848	0.593	0.746	0.781	0.07%	0.18%	0.03%	0.03%	**0.08%**
	Tibia anatomy	0.051	0.002	0.000	0.000	8.84%	9.31%	57.59%	95.76%	**42.88%**

the regions when introducing a 5°* posterior slope (−13.9% in MP; −27.5% in LP; −23.2% in MD; −10.1% in LD) (Fig. 4).

The tray material composition had a much smaller influence compared to the other factors (Fig. 4). The SED slightly increased in the proximal regions (+1.4% for GT; +3.4% for DKB; +1.2% for SD) under the baseplate and decreased under the stem when using Ti6Al4V instead of CoCrMo (Fig. 5f).

3.4. Absolute SED distributions (Normal vs. shelf tibia)

Substantial differences in SED distributions were seen posteriorly (Fig. 6, highlighted by black circles) between the normal and shelf tibia. For the normal tibia, the SED was continuously distributed along the bony wall posterior to the tray stem (Fig. 6d) (minimum wall thickness was 4.7-mm, excluding cement layer), whereas the SED had interruption at the same region for the shelf tibia (Fig. 6e) (minimum wall thickness was 2.2-mm). The SED interruption was improved when introducing a 5°* tibial posterior slope to the shelf tibia (Fig. 6f) (minimum wall thickness 3.6-mm).

*NOTE: A posterior slope of 5 – 7° is recommended in the manufacturer's surgical technique for the cruciate retaining version of Attune to provide proper PCL tension.

4. Discussion

Bone remodeling after total knee arthroplasty is regulated by the changes in strain energy density [6]. In this study, we investigated post-operative bone strains during gait, stair descent, and deep knee bending activities. Specifically, we assessed the impact of surgical alignment, tray material properties, posterior cruciate ligament balance, tray posterior slope, and patient anatomy (tibial posterior overhang) on strain energy density distributions in the proximal tibia. The variations in femoral-insert contact locations and contact force directions due to surgical alignment, tray posterior slope, and PCL balancing were considered. We also included patellar tendon and PCL forces when calculating SED distributions.

The impact of tibial geometry on SED was substantial. To enable better comparisons, these two tibiae were selected due to their similar size and were implanted with the same-size prosthesis. The SED changes in distal regions were larger than those changes in proximal regions. The small differences proximally were mainly due to the changes in ligament force locations (different ligament attachment sites for each tibia). In the distal ROIs, the shelf tibia had less remaining bone stock posteriorly, which modified load transfer and minimized SED compared to the normal tibia. In addition, the shelf tibia showed interrupted SED distribution with no posterior slope (Fig. 6) whereas the normal tibia had continuous SED distribution, indicative of potential bone loss in that region. Introducing a 5° posterior slope increases the posterior wall thickness (Fig. 6f) with this anatomy/implant combination and should be chosen to maximize fixation, as well as staying within the manufacturer's recommended surgical technique.

It is useful to examine the mechanisms that create changes in SED for PCL balance, surgical alignment, and posterior slope factors. A five percent increase in PCL tightness increased PCL forces by 84% during DKB activity, which also restricted the femur sliding anteriorly with respect to the tibia (Fig. 2c). The total peak joint loads were increased by an average of 168 N (7.9%). The increase in SED in all the regions during DKB activity was mainly caused by these increased femoral-insert contact forces. Alignment changed the medial and lateral contact force distribution significantly, but the total joint contact forces were fairly consistent. During GT and SD, peak medial contact forces decreased by 11.4%, and peak lateral contact forces increased by 11.8% when selecting mechanical instead of anatomic alignment. This led to the SED decrease in the medial and increase in the lateral ROIs. When a 5° posterior slope was introduced in GT and SD activities, the total joint contact forces (<2.0%) and the medial-lateral distributions (<1.5%) were nearly unchanged. However, the medial-lateral contact locations shifted about 2.2 mm posteriorly (Fig. 2b). The change in SED (increased posteriorly and decreased anteriorly) was mostly due to the changes in the joint contact locations and force directions. For the DKB activity, the total femoral-insert contact forces decreased by an average of 5.5% (144 N), which resulted in decreased SED over all regions. The resulting strain changes for these three factors were mainly due to these changes in the joint contact and soft tissue loads. It should also be noted that ranking of the most influential factors is clearly dependent on the variability chosen for each.

It can be concluded that the SED in the proximal tibia would increase only when the joint contact load increased (in this study, only achieved from a tighter PCL). According to the manufacturer, a tight PCL should be avoided to enable proper implant kinematics, however, minimizing the reduction in SED may be achieved through other surgical parameters. Previous studies demonstrated that medial tibial bone loss is most common [26, 27]. A recent publication also reported that the medial region generally showed a larger decrease in SED relative to the lateral region after TKA [28], which indicated that the bone loss would most likely occur at the proximal-medial tibia under the baseplate. Thus, an anatomic alignment may be preferred, as it would result in considerably increased SED in the medial region compared with mechanical alignment. The tray posterior slope influences the SED anterior-posterior distribution only moderately, however, this is a key factor that determines the minimum thickness of the remaining posterior wall after TKA. These findings have clinical implica-

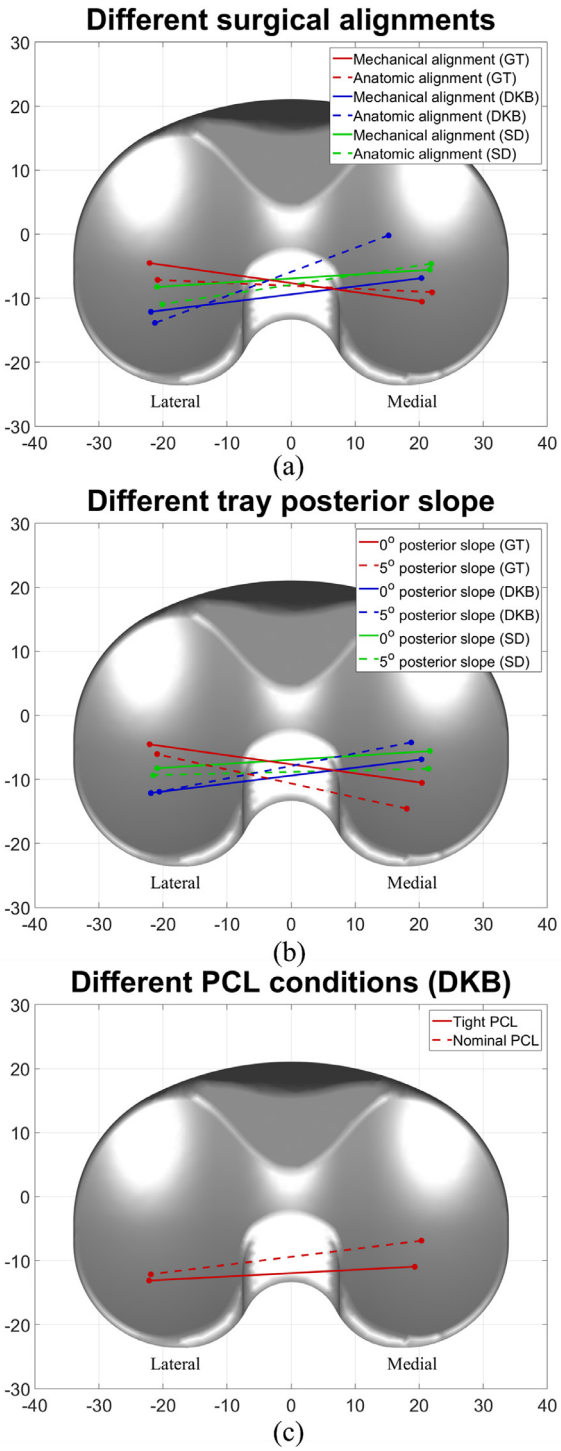

Fig. 2. Femoral-insert contact locations at the peak loading frames under different surgical alignments, tray posterior slopes, and PCL balancing conditions. Results were derived from the lower limb model. *Note that for GT and SD, the PCL balancing conditions have no effect on femoral-insert contact since the PCL was slack during these two activities (Fig. 2c). ***(color should be used for this figure)***.

tions. When deciding the best approach for a specific patient, we recommend choosing the tray alignment configuration based on a patient-specific evaluation of geometry and bone quality. For example, an anatomic alignment in the frontal plane is likely preferred to minimize stress shielding and the change in strain from the native state on the medial side. We also recommend introducing a tray posterior slope according to the patient's tibial anatomy

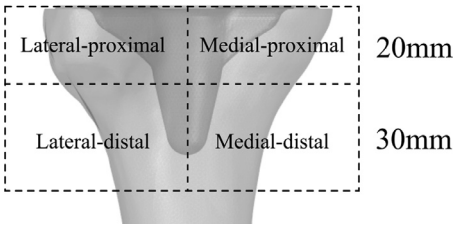

Fig. 3. Region divisions of the proximal tibia.

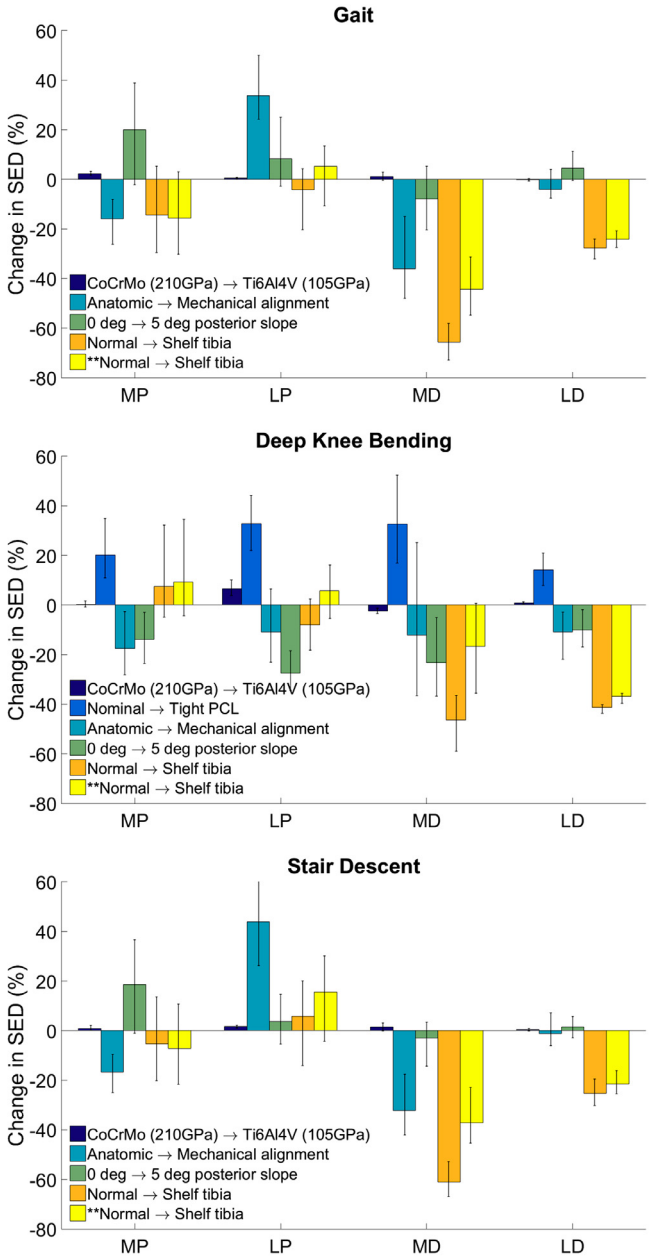

Fig. 4. The overall change in SED for five comparison pairs: tray materials (Ti6Al4V and CoCrMo), PCL conditions (tight and nominal), surgical alignments (mechanical and anatomical), tray posterior slopes (0° and 5°), and tibial anatomy (shelf and normal). ** *indicates that the same material properties were used for the normal and shelf tibiae and the results were normalized with respect to tibial regional volumes.* ***(color should be used for this figure)***.

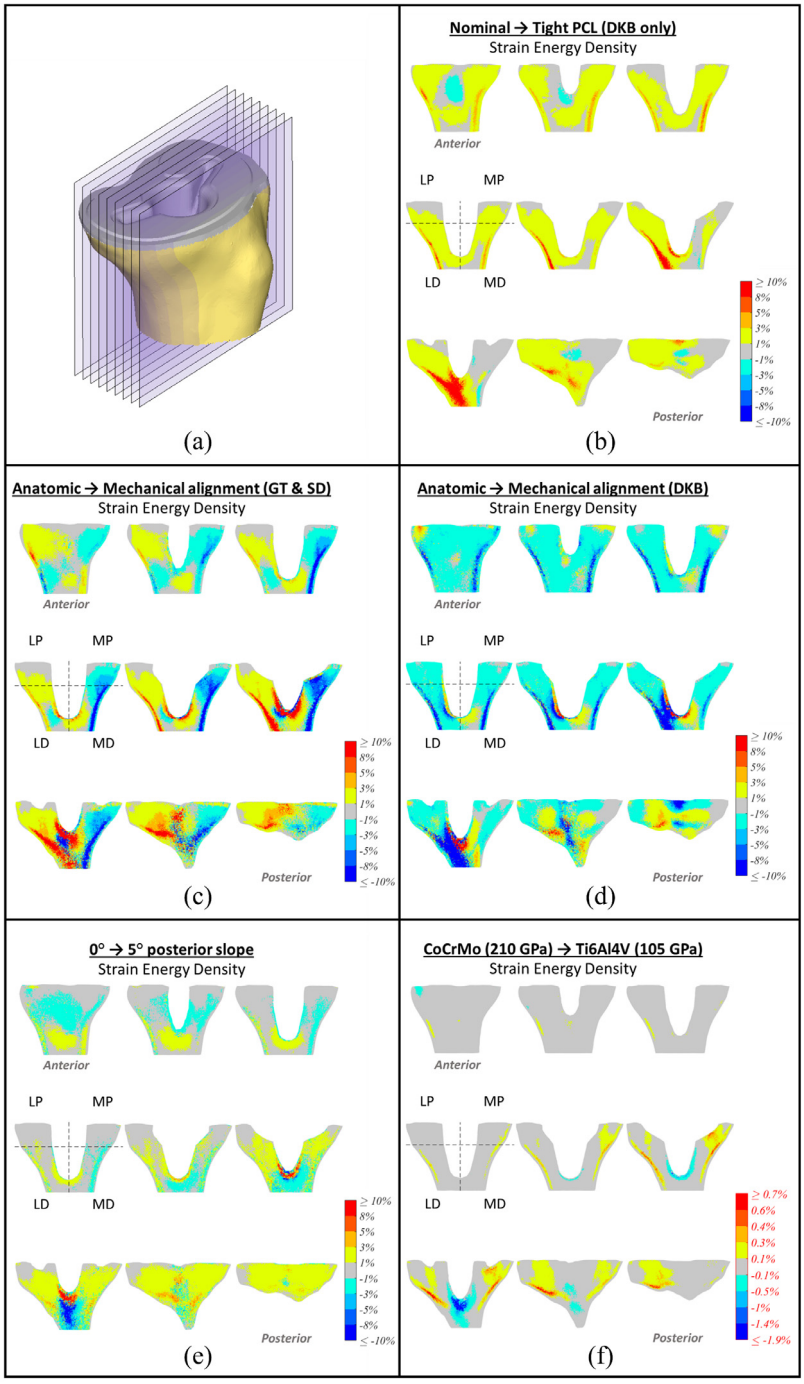

Fig. 5. Contour maps of the changes in SED for each of the factors studied. (a) Cross-section divisions; (b) PCL balance (DKB only); (c) Surgical alignment (GT & SD); (d) Surgical alignment (DKB); (e) Tray posterior slope; (f) Tray materials. (*The normal tibia was used for the plots; the shelf tibia has similar results*). ***(color should be used for this figure)***.

to keep the posterior wall thickness, avoid stem-cortex contact, and best mimic tibial strain. A slightly tighter PCL might be desired if the overall bone quality is poor, as this would increase the compressive contact loading, which results in increased SED across the proximal tibia.

It has been previously discussed that the tray material composition causes stress shielding of periprosthetic bones [26]. In this study, we found that the impact of tray material properties on post-operative SED distribution was negligible, especially when compared with changes found for typical patient and surgical variables. An average of 1.6% SED difference was found in the proximal tibia when comparing using CoCrMo and Ti6Al4V as the tray material. This finding is in line with a previous study that showed no differences in stress shielding when using titanium and cobalt-chrome tibial prostheses [29].

This study has limitations to note. Although we addressed the impact of anatomy of two tibial types, only two tibiae were included in this study. Matching the material properties of the two tibiae helped to understand the relative impact of material and geometry, but future studies should focus on a more comprehensive distribution of patient anatomy. It is clear that not only the tibial posterior overhang and densities vary between subjects, but

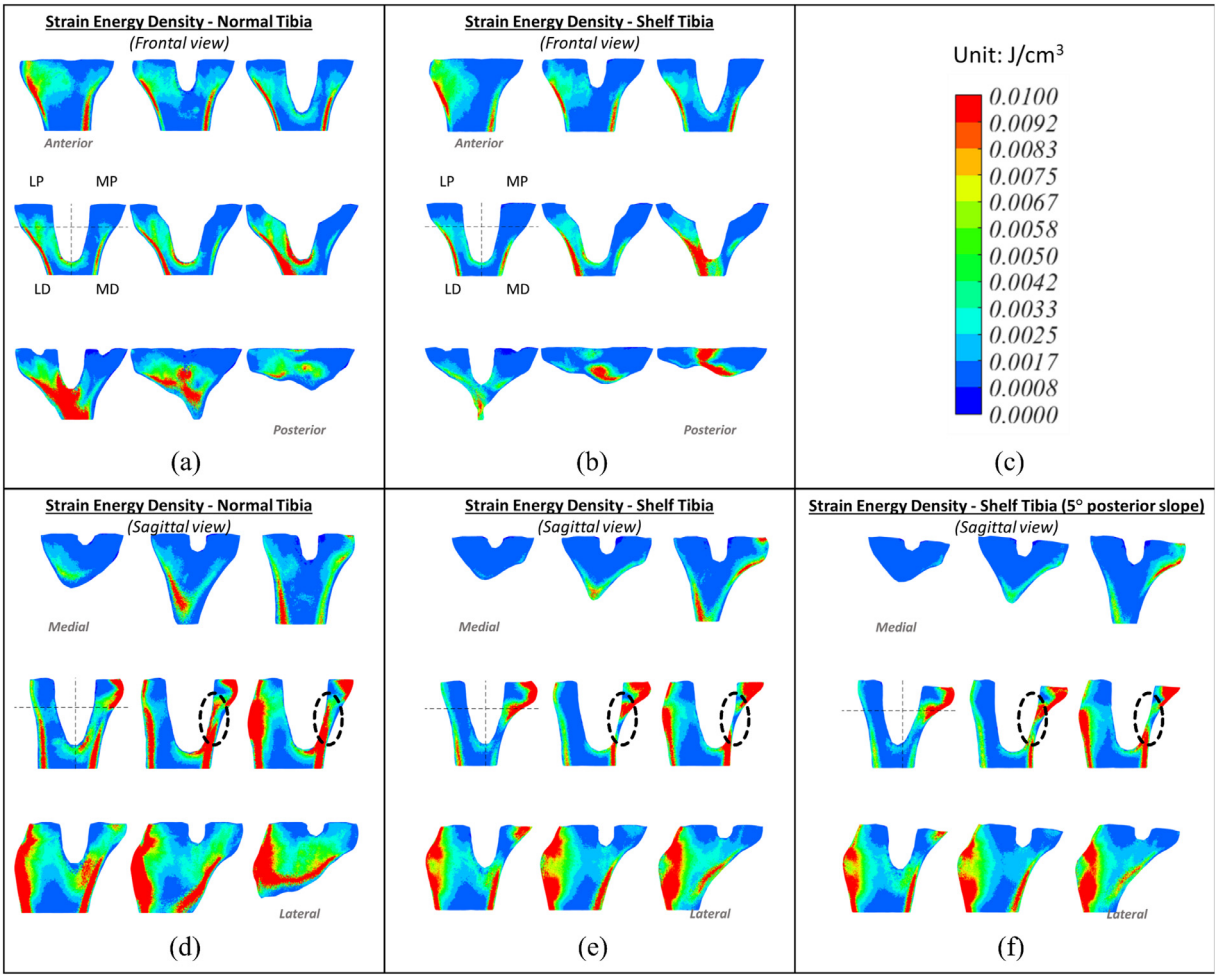

Fig. 6. Contour maps of the bone SED distributions in the frontal and sagittal plane. (a & d) Normal tibia with 0° posterior slope; (b & e) Shelf tibia with 0° posterior slope; (f) Shelf tibia with 5° posterior slope; (*Representative configuration used for the plots: mechanical alignment, 0 or 5° posterior slope, nominal PCL condition, and CoCrMo tray material during deep knee bending activity*). ***(color should be used for this figure)***.

also the bone geometry and material distribution, patient weight, and other knee-related anatomical features (such as Q-angle, ligament attachment sites, and hip-knee-ankle angle) are different. The complex combination of these anatomical factors would alter the ligament forces, contact conditions, tibial moments, etc., and finally SED distributions. However, we believe that the primary impacts and trends of the factors on SED distributions will be still valid under those situations (for example, a tighter PCL would increase the overall SED, and an anatomic alignment would result in more SED in the medial region comparing with a mechanical alignment, etc.). The cemented implant was assumed here to be perfectly bonded at the tray-bone interface, which is a simplification of the variation likely seen in vivo. Only one implant design (cemented, fixed-bearing, cruciate-retaining) was tested in this work. The loading patterns and strain distributions may be different for other implants, especially with different tray designs. Finally, the bone strain analysis performed in this study cannot be reproduced and examined experimentally. However, in the study immediately preceding the current, prediction of tibial surface displacement was validated experimentally with digital image correlation and a known, physiological loading condition for several tibial specimens [30]. Models were developed using the same process for representing bony mechanics. In that study, three cadaveric tibial specimens were physically tested under GT, DKB, and SD loads, while digital image correlation (DIC) was used to measure tibial surface displacement. Corresponding computational models were developed using the same methods shown here. The Root-Mean-Square differences and Pearson's correlations between experimentally measured surface displacements and predictions were 78.9 μm and 0.84 [30].

In summary, the potential differences in post-operative proximal tibial SED distributions for five typical TKA parameters were evaluated. Tibial anatomy was found to have the largest impact on post-operative bone strains. The impact of PCL balancing, surgical alignment, and tray posterior slope were considerable. The SED changes for these three factors were mainly due to the changes in loading conditions. Among those, PCL balancing affects the overall strain energy magnitude, whereas the alignment and posterior slope primarily influence the medial-lateral and anterior-posterior SED distributions, respectively. The impact of tray material modification was much smaller than the aforementioned factors. The results indicated that maximizing post-operative fixation is possible using optimized surgical parameters in the frontal plane as well as posterior slope to address patient anatomy.

Declaration of Competing Interest

Authors (PR, CC) received research or institutional support as a principal investigator from DePuy Synthes Products, LLC.

Acknowledgments

This study was funded by DePuy Synthes Products, LLC.

Funding

DePuy Synthes Products.

Ethical approval

Not required.

References

[1] Leichtenberg CS, Vliet Vlieland TP, Kroon HM, et al. Self-reported knee instability associated with pain, activity limitations, and poorer quality of life before and 1 year after total knee arthroplasty in patients with knee osteoarthritis. J Orthop Res 2018;36:2671–8. doi:10.1002/jor.24023.
[2] Sloan M, Premkumar A, Sheth NP. Projected volume of primary total joint arthroplasty in the U.S., 2014 to 2030. J Bone Jt Surg 2018;100:1455–60. doi:10.2106/jbjs.17.01617.
[3] Dalury DF, Pomeroy DL, Gorab RS, Adams MJ. Why are total knee arthroplasties being revised? J Arthroplast 2013;28:120–1. doi:10.1016/j.arth.2013.04.051.
[4] edited by Wolff J. In: Maquet P, Furlong R, editors. Berlin: Springer-Verlag; 1892. edited by p. 1986.
[5] Frost HM. Perspectives: the role of changes in mechanical usage set points in the pathogenesis of osteoporosis. J Bone Miner Res 1992;7:253–61. doi:10.1002/jbmr.5650070303.
[6] Ruimerman R, Rietbergen BV, Hilbers P, Huiskes R. The effects of trabecular-bone loading variables on the surface signaling potential for bone remodeling and adaptation. Ann Biomed Eng 2005;33:71–8. doi:10.1007/s10439-005-8964-9.
[7] Burger EH, Klein-Nulend J. Mechanosensory transduction in bone—Role of the lacuno-canalicular network. FASEB J 1999;13:S101–12. doi:10.1096/fasebj.13.9001.s101.
[8] Scott CEH, Biant LC. The role of the design of tibial components and stems in knee replacement. J Bone Jt Surg Br 2012;94:1009–15. doi:10.1302/0301-620x.94b8.28289.
[9] Completo A, Fonseca F, Simões JA. Finite element and experimental cortex strains of the intact and implanted tibia. J Biomech Eng 2007;129:791–7. doi:10.1115/1.2768382.
[10] Zhang QH, Cossey A, Tong J. Stress shielding in periprosthetic bone following a total knee replacement: effects of implant material, design and alignment. Med Eng Phys 2016;38:1481–8. doi:10.1016/j.medengphy.2016.09.018.
[11] Innocenti B, Truyens E, Labey L, et al. Can medio-lateral baseplate position and load sharing induce asymptomatic local bone resorption of the proximal tibia? A finite element study. J Orthop Surg Res 2009;4:26. doi:10.1186/1749-799x-4-26.
[12] Jia Z, Gong H, Hu S, et al. Influence of design features of tibial stems in total knee arthroplasty on tibial bone remodeling behaviors. Med Eng Phys 2017;48:103–13. doi:10.1016/j.medengphy.2017.06.046.
[13] Simpson D, Price A, Gulati A, et al. Elevated proximal tibial strains following unicompartmental knee replacement—a possible cause of pain. Med Eng Phys 2009;31:752–7. doi:10.1016/j.medengphy.2009.02.004.
[14] Perillo-Marcone A, Taylor M. Effect of Varus/valgus malalignment on bone strains in the proximal tibia after TKR: an explicit finite element study. J Biomech Eng 2006;129:1–11. doi:10.1115/1.2401177.
[15] Duda GN, Heller M, Albinger J, et al. Influence of muscle forces on femoral strain distribution. J Biomech 1998;31:841–6. doi:10.1016/s0021-9290(98)00080-3.
[16] Ko DO, Lee S, Kim KT, et al. Cement mantle thickness at the bone cement interface in total knee arthroplasty: comparison of PS150 RP and LPS-flex knee implants. Knee Surg Relat Res 2017;29(2):115–21. doi:10.5792/ksrr.16.013.
[17] Rho JY. An ultrasonic method for measuring the elastic properties of human tibial cortical and cancellous bone. Ultrasonics 1996;34(8):777–83. doi:10.1016/S0041-624X(96)00078-9.
[18] Kaneko TS, Bell JS, Pejcic MR, et al. Mechanical properties, density and quantitative CT scan data of trabecular bone with and without metastases. J Biomech 2004;37:523–30. doi:10.1016/j.jbiomech.2003.08.010.
[19] Anderson MJ, Keyak JH, Skinner HB. Compressive mechanical properties of human cancellous bone after gamma irradiation. J Bone Jt Surg 1992;74:747–52. doi:10.2106/00004623-199274050-00014.
[20] Fitzpatrick CK, Baldwin MA, Clary CW, et al. Evaluating knee replacement mechanics during ADL with PID-controlled dynamic finite element analysis. Comput Methods Biomech Biomed Eng 2014;17:360–9. doi:10.1080/10255842.2012.684242.
[21] Kutzner I, Heinlein B, Graichen F, et al. Loading of the knee joint during activities of daily living measured in *vivo* in five subjects. J Biomech 2010;43:2164–73. doi:10.1016/j.jbiomech.2010.03.046.
[22] Pfitzner T, Moewis P, Stein P, et al. Modifications of femoral component design in multi-radius total knee arthroplasty lead to higher lateral posterior femoro-tibial translation. Knee Surg Sports Traumatol Arthrosc 2017;26:1645–55. doi:10.1007/s00167-017-4622-7.
[23] Escamilla RF, Macleod TD, Wilk KE, et al. Cruciate ligament loading during common knee rehabilitation exercises. Proc Inst Mech Eng H 2012;226:670–80. doi:10.1177/0954411912451839.
[24] Hensler D, Musahl V, Illingworth KD, et al. The function of the two bundles of the posterior cruciate ligament – an in-vivo study using dynamic stereo X-ray system (DSX). In: Proceedings of the ORS 2012 annual meeting; 2012. Poster No. 2297.
[25] Navacchia A, Sintini I, Rullkoetter PJ. Effects of TKR alignment, implant design and patient pre-operative alignment on post-operative proximal tibia strain. ISTA; 2018.
[26] Martin JR, Watts CD, Levy DL, et al. Tibial tray thickness significantly increases medial tibial bone resorption in cobalt–chromium total knee arthroplasty implants. J Arthroplasty 2017;32:79–82. doi:10.1016/j.arth.2016.06.007.
[27] Yoon C, Chang MJ, Chang CB, et al. Medial tibial periprosthetic bone resorption and its effect on clinical outcomes after total knee arthroplasty: cobalt-chromium vs titanium implants. J Arthroplasty 2018;33:2835–42. doi:10.1016/j.arth.2018.04.025.
[28] Anijs T, Wolfson D, Verdonschot N, Dennis J. Population-based effect of total knee arthroplasty alignment on simulated tibial bone remodeling. J Mech Behav Biomed Mater 2020;111:104014. doi:10.1016/j.jmbbm.2020.104014.
[29] Completo A, Talaia P, Fonseca F, Simões J. Relationship of design features of stemmed tibial knee prosthesis with stress shielding and end-of-stem pain. Mater Des 2009;30:1391–7. doi:10.1016/j.matdes.2008.06.071.
[30] Yang H, Bayoglu R, Sharifi Ravani M, et al. Validation and sensitivity of model-predicted proximal tibial displacement and tray micromotion in cementless total knee arthroplasty under physiological conditions. J Mech Behav Biomed Mater 2020;109:103793. doi:10.1016/j.jmbbm.2020.04.103793.